Available at www.scientevents.com/proscience/
ScientEvents
ProScience 3 (2016) 84-93
ProScience

Conference Proceedings
2nd International Conference on Atmospheric Dust - DUST2016

Atmospheric dynamics of the Harmattan surge in March 2, 2004

Ashok Kumar Pokharel[1*], Michael L. Kaplan[1], Stephanie Fiedler[2]

[1]*Division of Atmospheric Sciences, Desert Research Institute, Reno, USA*
[2]*Max-Planck-Institute for Meteorology, Hamburg, Germany*
[*]*ashokpokharel@hotmail.com*

Abstract

Meso-α/β scale observational and meso-β/γ scale numerical model analyses were performed to study the atmospheric dynamics responsible for generating Harmattan dust storm. For this dust storm case study, MERRA reanalysis datasets, WRF simulated very high resolution datasets, MODIS/Aqua and Terra images, EUMETSAT images, NAAPS aerosol modelling plots, surface observations, and rawinsonde soundings were analyzed. The analysis of this dust storm shows (1) the presence of a well-organized baroclinic synoptic scale system, (2) this dust storm composed of two dust storm events, (3) small scale dust emission events (first dust storm event) which occurred prior to the formation of the primary large-scale dust storms (second dust storm event), (4) cross Atlas Mountain flows which produced a strong leeside inversion layer prior to the large scale dust storm, (5) the presence of thermal wind imbalance in the exit region of the mid-tropospheric jet streak in the lee of the Atlas Mountains shortly after the time of the inversion formation, (6) major dust storm formation was accompanied by large magnitude ageostrophic isallobaric low-level winds as part of the meso-β scale adjustment process, (7) substantial low-level turbulence kinetic energy (TKE), and (8) the emission of the dust occurred initially in narrow meso-β scale zones parallel to the mountains, and later reached the meso-α scale when suspended dust was transported away from the mountains. In addition to this there were additional meso-β and meso-γ scale adjustment processes resulting in Kelvin waves and the thermally-forced MPS circulation, respectively. The Kelvin wave preceded a cold pool accompanying the air behind the large scale cold front instrumental in the major dust storm. The Kelvin wave organized the major dust storm in a narrow zone parallel to the mountains before it expanded upscale (meso-α to synoptic scale). The thermally-forced meso-γ scale adjustment processes, which occurred in the canyons, resulted in the numerous dust streaks leading to the entry of the dust into the atmosphere due to the presence of significant vertical motion and the TKE generation. This indicates that there were meso-β to meso-γ scale adjustment processes at the lower levels after the imbalance within the exit region of the upper level jet streak and these processes were responsible for causing this large scale dust storm (synoptic scale).

Keywords: Jetlet; Thermal ridge; Jet adjustment; Ageostrophic/isallobaric wind; Vorticity; TKE

ISSN: 2283-5954
Selection and peer-review under responsibility of DUST2016 Scientific Committee
DOI:10.14644/dust.2016.014

1. Introduction & methods

There are major dust event sources in North Africa, Arabian Peninsula, Iran, Pakistan, Afghanistan, Turkmenistan, the Kalahari desert, Tarim Basin in China, and Northern India (Engelstaedter et al., 2006). The Sahara, which lies in North Africa, represents a major subtropical desert, covering the Western Sahara, Morocco, large parts of Algeria, Mauritania, Mali, Niger, Libya, Chad, Egypt, Sudan, and Tunisia, and represents the most prolific aeolian dust source in the world (Prospero et al., 2002; Washington et al., 2003). The Sahara desert is dominated most of the year by the northeasterly wind-driven dry and hot air originating from the anticyclonic system centered over the North Atlantic Ocean (Shao, 2000). Ozer (2001) found that the maximum frequency of dust storms over West Africa occurs during the period of local 9:00 to 15:00 hrs due to the enhancement of dry convection in the planetary boundary layer during the day and minimum frequency in the night between local 21:00 hrs and 3:00 hrs. During the northern hemisphere cold season (November to April), the West African climate is influenced by the northeasterly trade wind system called the Harmattan, which is developed by the meridional pressure gradients at the synoptic scale across the Saharan desert (Burton et al., 2013). Kalu (1979) stated the generation of a strong Harmattan wind is caused by the sudden intensification of the subtropical anticyclone in association with a pressure surge over the Sahara, significant low-level wind speeds, and a cold outbreak from the Mediterranean Sea. Fiedler et al.(2015) showed that synoptic scale cold air advection over North Africa causes the Harmattan surges. In the regional climate system, the importance of the study of the Harmattan wind system has been increasing since it advects a significant amount of mineral dust equatorwards across the region causing severe winter weather conditions as well as a wide range of negative impacts on visibility, agriculture, and human health (Kalu, 1979; Burton et al., 2013). These data combined with previous findings indicate that to discover the origin of West African dust storms, a detailed understanding of the multi-scale dynamical/thermodynamical processes are the key factors. Though there are many studies about the impacts and transport of Saharan dust in various parts of Africa there is much less research that exists describing the mesoscale atmospheric processes, which are mainly responsible for creating the severe dust storms as indicated by the lack of relevant published data from this region.

1.1 Hypotheses

As this particular Harmattan dust storm of March 2, 2004 was observed in the leeward of the Atlas Mountains, it was hypothesized that this dust storm was associated with the evolution of ageostrophic motions due to the precursor Atlas Mountains thermal perturbation/inversion and its interaction with a large background/upstream propagating jet streak. This interaction first manifested itself on the lee of the Atlas Mountains. The leeside mass perturbation indicated by mountain waves, caused by the development and blocking of the inversion layer, led to the development of a thermally direct ageostrophic circulation pattern and mesoscale vertical motion when the core of the polar jet streak approached the mountains. This thermally direct circulation developed in response to the geostrophic imbalance across the exit region of the upper level jetstreak. Besides the large scale jet streak imbalance, it was also hypothesized that this particular dust storm was associated with the terrain-induced local effects.

1.2 Methodology

Satellite imagery from Meteosat-8 provided by the European Organization for the Exploitation of Meteorological Satellites (EUMETSAT), Moderate Resolution Imaging

Spectroradiometer (MODIS)/Aqua and Terra (level 1b, collection 51, 1 km resolution, and RGB composite), rawinsonde soundings from the University of Wyoming, and aerosol optical depth imagery captured by the MODIS/Aqua instrument (level 3 daily (D3) and collection 6) were collected. Besides this, observational surface data archived by Weather Underground (e.g., Bechar, Tindouf, Adrar, and Timimoun surface stations in Algeria and Nouakchott station in Mauritania) and evolution of the dust by an aerosol modeling system at 1º X 1º horizontal resolution from the Navy Aerosol Analysis and Prediction System (NAAPS) were also taken into account. For the synoptic to meso-scale observational atmospheric processes analysis, the reanalysis data set of surface pressure, geopotential height, air temperature, wind speed and direction, vertical motion, vertically integrated atmospheric mass tendency, and kinetic energy due to pressure gradient force obtained from the Modern Era Retrospective-Analysis for Research and Applications (MERRA) were used to make horizontal cross sections. Vertical cross sections of u- wind speed (west-east wind speed), v-wind speed (north-south wind speed) components, and potential temperature were also plotted from the MERRA data sets. This MERRA has 0.50º X 0.67º horizontal resolution data sets for the surface to different pressure levels (i.e. 925, 850, 700, 500 hPa) in 1-hourly and 6-hourly intervals. In the beginning of the analysis, the MERRA products were analyzed to gain the general overview of the atmospheric conditions at the larger scales. However, because they were limited in spatial and temporal resolution these products were not able to reveal the exact time and area of the jet's imbalance condition and the accompanying evolution of ageostrophic motions, spatial scale estimates of the vertical motions, and associated cooling in the mid-tropospheric levels. Because of these limitations of the MERRA, at the meso-β scale, i.e., to achieve better accuracy of the analysis of the atmospheric processes in finer spatial and temporal resolution, such as time periods of geostrophic imbalance and adjustment processes during the occurrence of the dust storms, the Weather Research and Forecasting (WRF) model (non-hydrostatic mass core model) (Skamarock et al., 2008), was run over the region employing National Centers for Environmental Prediction (NCEP)/Global Forecasting System (GFS) products.

2. Data analyses

2.1 Simulation experiment overview

In order to better understand mesoscale dynamics instrumental in dust storm formation, the Weather Research and Forecasting model (WRF) (non-hydrostatic mass core model) was utilized (Skamarock et al., 2008) over the region employing NCEP/GFS products (1° resolution) for initialization and lateral boundary conditions. Four WRF (Version 3.5.1) modeling domains were used in each case study. The WRF model was initialized over a parent domain, which had horizontal grid dimensions of 82 X 118 grid points (54 km horizontal grid spacing) in the west-east and north-south directions. Additionally, three domains were nested into the parent domain having 208 X 274 (18 km), 502 X 613 (6 km), and 802 X 802 (2 km) grid points. They were integrated in time for the following periods: 1200 UTC March 1 to 1800 UTC March 3 for the parent (first) domain, 1800 UTC March 1 to 1800 UTC March 3 for the second domain, 0000 UTC March 2 to 1800 UTC March 3 for the third domain, and 1200 UTC March 2 to 1800 UTC March 3 in 2004 for the fourth (innermost) domain. The model physics includes (i) momentum and heat fluxes at the surface using an Eta surface layer scheme (Janjić,1996, 2001) that follows Monin-Obukhov

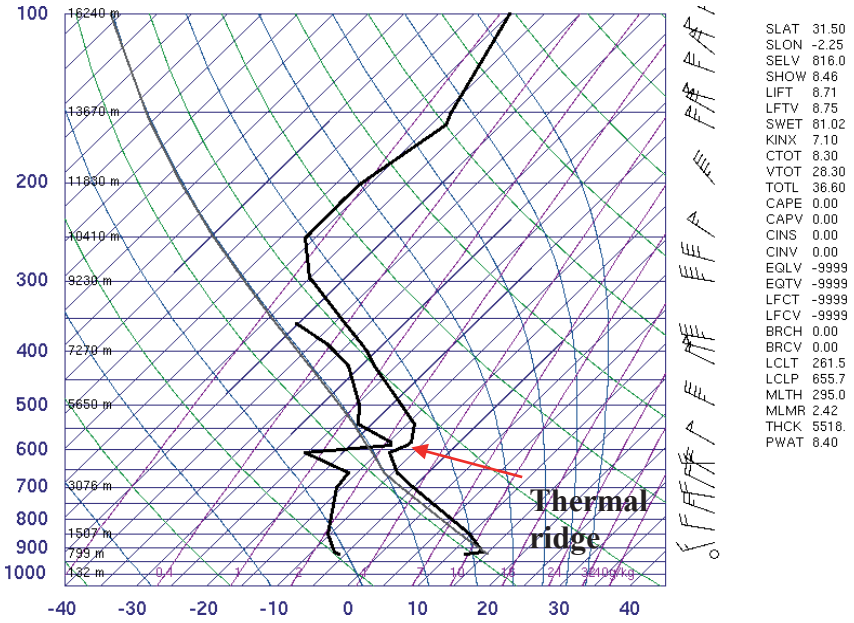

Fig. 1. Rawinsonde soundings on 0000 UTC March 2, 2004 at Bechar in Algeria (source: University of Wyoming)

similarity theory, (ii) turbulence processes following the Mellor-Yamada- Janjić 1.5 order (level 2.5) turbulence closure model (Mellor and Yamada, 1974; Janjić,2001), (iii) convective processes following the Betts-Miller-Janjić cumulus scheme (Betts,1986; Betts and Miller,1986; Janjić,1994) applied only on the 54 and 18 km grid, (iv) cloud microphysical processes following the Thompson double-moment scheme (Thompson et al., 2004, 2006), (v) radiative processes following the Rapid Radiative Transfer Model for long wave radiation (Mlawer et al., 1997) and Dudhia's scheme for short wave radiation (Dudhia,1989), and (vi) land-surface processes following the Noah land surface model (Noah LSM) (Chen and Dudhia, 2001; Ek et al., 2003).

2.2 Analyses of the first dust storm event

On the early part on March 2, 2004 the air adjacent to the bottom of the lee slope of the south/southwestern edge of the Atlas Mountains was quite warm, which was indicative of a downslope wind and the advection of the residual well-mixed convective planetary boundary layer from the previous afternoon which formed above the Atlas Mountains. This elevated mixed layer (EML) was confirmed from observed soundingsat Bechar located in the leeside of the Atlas (Fig. 1, Fig. 2), WRF 6km vertical cross sections of isentropic surfaces, and the horizontal cross sections of 850 hPa and 925 hPa of wind speed/direction and temperature over the 25-31°N 3-10°W at 0000-0600 UTC on March 2. This downslope compressed layer had a deep dry adiabatic lapse rate in the early morning hours on March 2 consistent with the sounding data at Bechar and also consistent with overturning isentropes. With surface heating during the early morning solar cycle there was an increase in the convective turbulence even with relatively weak wind conditions which facilitated the generation of the dust from the surface at 0600 UTC over the ~25-29°N 9-6°W region as also shown in a case study in Klose and Shao (2013).This is consistent with the dust evolution in the NAAPS plot. After 0600 UTC, as the solar heating started to increase, the air adjacent to the bottom of the lee slope at

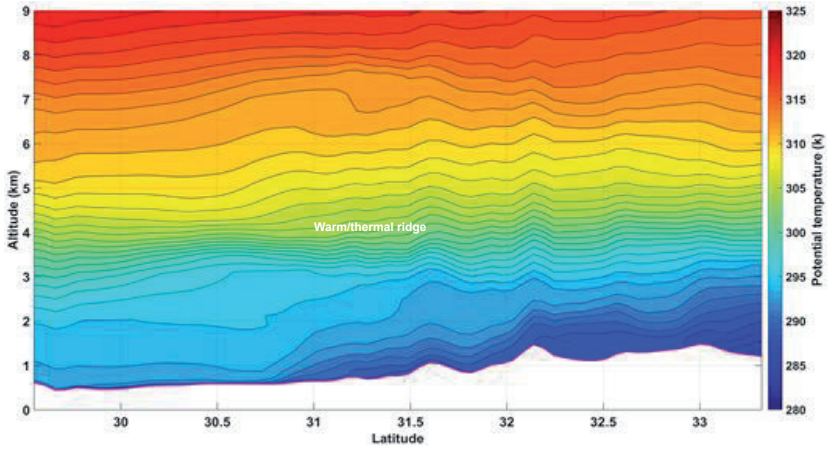

Fig.2. Vertical cross sections of potential temperature at 2°W at 0000 UTC on March 2, 2004 (6 km resolution WRF product)

the mountain range became cooler relative than air over the upper parts of the slope of mountain range (Zhang and Koch, 2000). This led to the flow of lower level air from the bottom of the Atlas towards the top, i.e., from high pressure at the bottom to low pressure at the top/cool to warm advection of air up the mountain. This is a reversed air flow towards the top of the Atlas (Atkinson, 1981; Banta,1984). This thermally-forced phenomenon represents the formation of a mountain plains solenoid circulation (MPS) (Wolyn and McKee, 1994). As the process continued during the late morning, there was the development of the strong upward folding of the isentropic surface at the Atlas ridge top which subsequently accelerated the airflow towards the east outward from the MPS (Banta,1984). This resulted in vertical wind shear (Fig. 3) with increasing west-northwesterly flow above the valley towards the east of the Atlas Mountains overrunning air advected from the southwest. When this horizontally-directed accelerative airflow interacted with the vertically stretched isentropes in the warm air column (e.g. statically unstable environment) to the south/southeastward of the Atlas, which had a substantial mixing depth, shown by the vertical

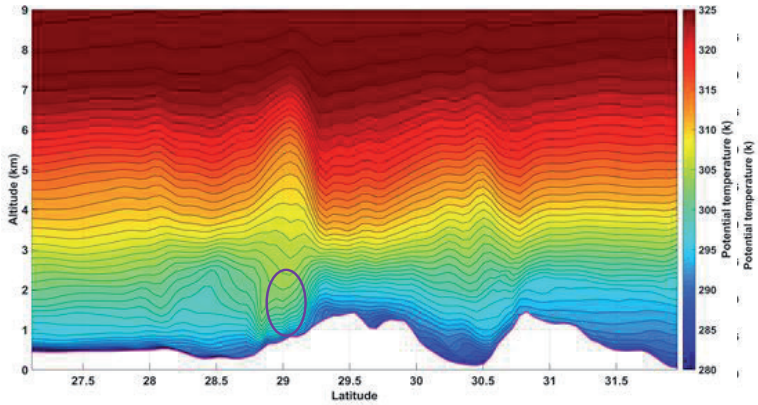

Fig. 3. Vertical cross sections of potential temperature at 9.12°W on 0600 UTC March 2, 2004 (6 km resolution WRF product)

cross sections of the potential temperature and deep dry adiabatic lapse rate illustrated in the soundings as mentioned in the previous section, there was a generation of buoyant eddies. Consequently, this well-mixed circulation ablated the dust from the surface around 1200 UTC and afterwards on March 2 shown by the significant magnitudes of the turbulence kinetic energy (TKE). The evolution of the dust at this time period was comparatively higher than the earlier period with respect to areal strength due to the warming from the rise of sensible heating. This is consistent with the direction of the northwesterly/west-northwesterly wind flow during the occurrence of the first dust storm observed at Tindouf at 0900-1200 UTC and the image shown by the MODIS/Aqua at 1335 UTC on March 2, 2004.

2.3 Analysis of the second dust storm event based on jet dynamics perspective

A detailed analysis of the jet dynamics from the analysis of 18 and 6km WRF products show that there was an interaction of the exit region of the polar jet streak with a local thermally perturbed air mass on the leeward side of the Atlas Mountains. This is consistent with the analyses by Kaplan et al. (2012, 2013a-b) in a North American case study. The presence of the thermally perturbed air mass (inversion sloping down from the mountain towards the Earth's surface) in the lee of the Atlas was shown by the sinking of isentropic surfaces over the 30-32.5°N 4-2°W region. This was also shown by the stable thermal ridge above the deep dry adiabatic lapse rate early in the morning captured by the rawinsonde soundings at Bechar (Fig. 1) and the 6 km WRF simulated vertical cross sections of isentropic surfaces (Fig. 2). This mass/local thermal perturbation contributed to the generation of an ageostrophic jetlet at 0900 UTC on March 2, 2004 in the leeward side of the Atlas over the 30-32°N 6-2°W region as the jet encountered the perturbed thermal field (Fig. 4).

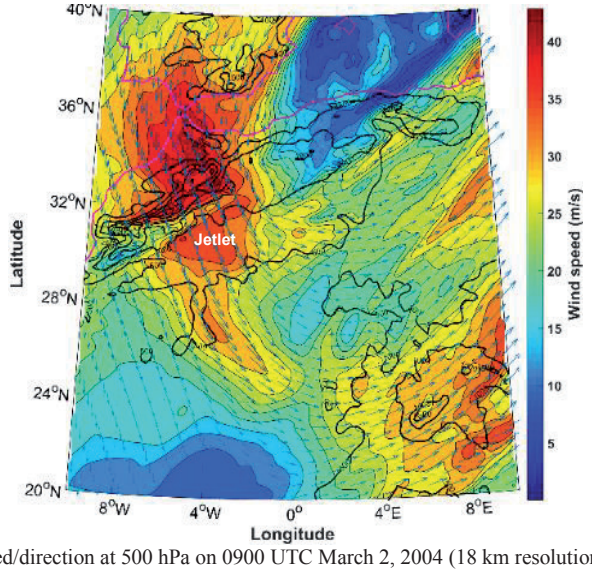

Fig. 4. Wind speed/direction at 500 hPa on 0900 UTC March 2, 2004 (18 km resolution WRF product)

After the interaction of the jet exit region of the jet with a local thermally perturbed air mass, winds were forced to increase above their geostrophic value. This led to the mass field adjustment modifying the wind field until it reaches to a new geostrophic balance. In this adjustment process, a thermally direct transverse ageostrophic circulation in the exit

region of the jetlet developed downstream from the mountain leading to the upward motion and the formation of the cold pool under the right exit of the jetlet (where velocity divergence exists). The development of the cooling was shown by the WRF soundings at 6 km horizontal resolution at 1400 UTC. This cold pool led to the rise of the low-level pressure creating an ageostrophic/isallobaric wind as a return branch of the direct circulation of the exit region of the jetlet at the lower levels (e.g., 925 hPa). This represents compensation in response to the adiabatic expansion/cooling of the rising parcels and their accompanying mass flux convergence. This low-level return branch ageostrophic wind accompanying the isallobaric ageostrophic flow (e.g., meso-β scale adjustment processes), which represented a southwestward-directed acceleration, advected the cold air generated

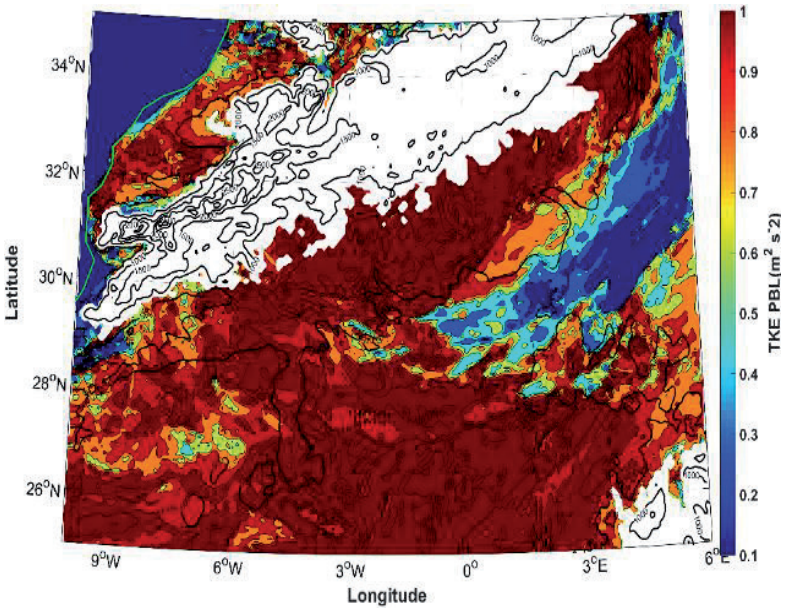

Fig. 5. Turbulent kinetic energy at 925 hPa on 1500 UTC March 2, 2004 (6 km resolution WRF product)

by the ascending flow westward/southwestward in the lee of the Atlas Mountains (upstream from the region of the jet streak imbalance) by 1500 UTC, where the deep cold air created a dry adiabatic/buoyant lapse rate extending downward from it. The interaction of this accelerating low-level ageostrophic wind with the layer of buoyant air column resulted in a favorable environment for turbulence kinetic energy (TKE) generation by buoyant eddies due to the summation of the wind shear and the buoyancy source terms in the TKE time tendency equation. After the generation of significant magnitudes of TKE (Fig. 5), there was a well-mixed circulation that is favorable for ablating dust from the surface. This is consistent with dust storms observed at Adrar, Bechar, and Timimoun and NAAPS simulation.

Similarly, in the meantime there was an additional meso-β scale mass field adjustment process revealed by the model. This was the result of the presence of the blockage of the cold air column by the mountain range and generation of the initial mass impulse. This mass build up by the jet adjustment process in the lower levels resulted in wind flow parallel to the mountains at 925 hPa by the ageostrophic isallobaric wind. This indicated the evolution of the Kelvin wave (Thomson,1879; Wang, 2002) on the northeast edge of the lee of the Atlas (33-35°N 3-6°E) at 1200 UTC on March 2. During the passage of time this

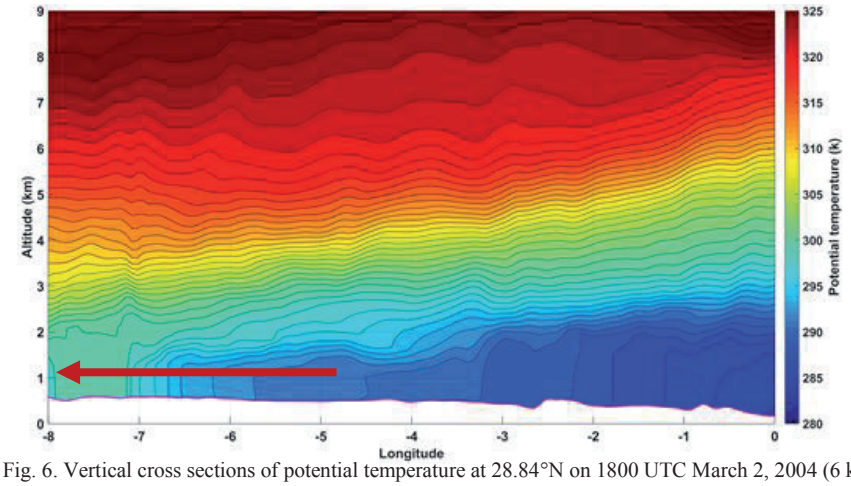

Fig. 6. Vertical cross sections of potential temperature at 28.84°N on 1800 UTC March 2, 2004 (6 km resolution WRF product)

northeasterly wind further strengthened and increased the dust emission. Afterwards, when this northeasterly wind, which had already significant momentum, interacted with the warm air column of vertically stretched isentropes developed by the MPS, which was present south/southwestward of the leeside of the Atlas Mountains as discussed above, there was a large production of the dust over the region on the south/southwest side of the Atlas. This Kelvin wave started to organize the dust storms after the early weak dust storm caused by the MPS circulation. The Kelvin wave subsequently intensified the dust storm resulting in its growth upscale by first concentrating its energy in a narrow zone adjacent to the lee of the mountains in the afternoon on March 2 before it expanded over time as a suspension of dust in the atmosphere by the growing wind perturbation orthogonal to the Kelvin wave. It is also seen that the northeasterly wind accompanying the Kelvin wave expanded further with the arrival of the Q-G cold pool from the region north/northeast of the Atlas Mountains (Fig. 6). The presence of the low static stability on the south/southwestward sections of the Atlas Mountains was shown by the stretching of the potential temperature in the vertical cross section in the WRF simulations during dust storm genesis.

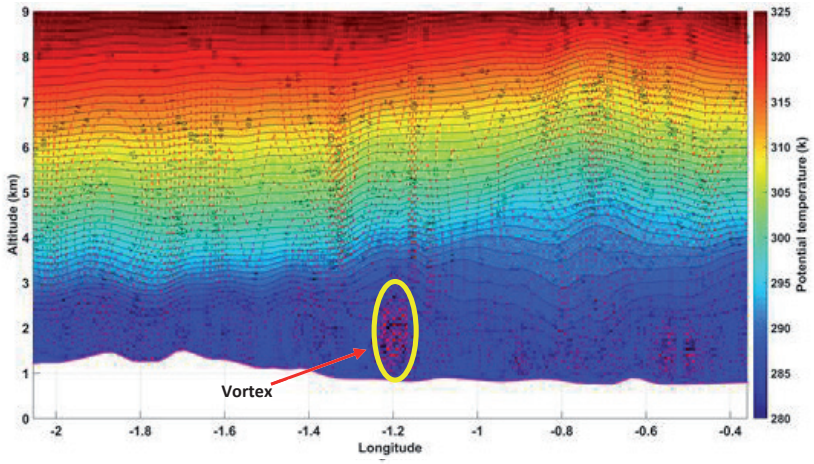

Fig. 7. Vertical cross sections of potential temperature at 32.07°N on 1330 UTC March 2, 2004 (2 km resolution WRF product)

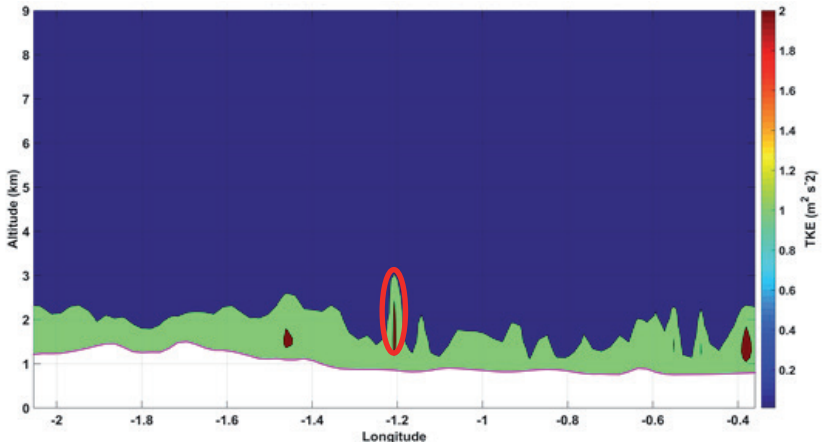

Fig. 8. Vertical cross sections of TKE at 32.07°N on 1330 UTC March 2, 2004 (2 km resolution WRF product)

These processes illustrated that the development of the northeasterly wind was associated with the huge cold surge and its interaction with warm air column on the south and southwestern edge of the Atlas Mountains as the Kelvin wave and quasi-geostrophic cold air surge merged in time. These processes led to the generation of the large volume of dust from large areas on the leeward side (south and southwest of the Atlas, 25-30°N 10°W-2°E) of the Atlas at around 2100 UTC on March 2 and afterwards. This is consistent with the sequential dust storms at Tindouf, Bechar, and Adrar during this time period. In the meantime, besides this meso-β scale adjustment processes, there were development of significant vertical motion, TKE, and vorticity, and their persistence in the leeside of the northeastern parts of the Atlas Mountains (~32°N 1.2°W) after the imbalance of the exit region of the polar jet streak (Fig. 7, Fig. 8). This is an indication of the typical meso-γ scale adjustment process.

This small scale adjustment process occurred when the cold air from the high pressure region of the bottom parts of a canyon was advected towards the thermally-forced (differential surface heating early in the day) low pressure area which formed in the upper parts of the canyon due to the differential of pressure. This upward flow shows the establishment of thermally direct circulation, which led to the generation of turbulence in the canyon after the reduction of the static stability due to the thermally-forced low pressure in the upper parts of the canyon. This led to an establishment of a well-mixed circulation resulting in a dust streak. This is a typical example of the generation of the dust streak with vortical characteristics from the MPS circulation. As this region occupies a number of canyons, this example of multiple meso-γ scale adjustment processes occurred in many of those canyons at that time period resulting in a widespread dust emission from this region.

3. Acknowledgments

We would like to thank to National Science Foundation (NSF) and National Center for Atmospheric Research (NCAR) for providing computational support.

References

Atkinson B.W. (1981). Meso-scale Atmospheric Circulations. Academic Press, 495 pp.

Banta R.M. (1984). Daytime boundary-layer evolution over mountainous terrain. Part I: Observations of the dry circulations. Monthly Weather Review 112, 340–356.

Betts A.K.(1986).Anew convective adjustment scheme. Part I: Observational and theoretical basis. Quarterly Journal of the Royal Meteorological Society 111, 1306-1335.

Betts A.K., Miller M.J. (1986). A new convective adjustment scheme. Part II: Single column tests using GATE WAVE, BOMEX, ATEX and Arctic air-mass data sets. Quarterly Journal of the Royal Meteorological Society 112, 693–709.

Burton R.R., Devine G.M., Parker D.J., Chazette P., Dixon N., Flamant C., Haywood J.M. (2013). The Harmattan over West Africa: nocturnal structure and frontogenesis. Quarterly Journal of the Royal Meteorological Society 139, 1364-1373.

Chen F., Dudhia J. (2001). Coupling an advanced land surface-hydrology model with the Penn State-NCAR MM5 modeling system. Part I: Model implementation and sensitivity. Monthly Weather Review 129, 569–585.

Dudhia J. (1989). Numerical study of convection observed during the Winter Monsoon Experiment using a mesoscale two-dimensional model. Journal of Atmospheric Sciences 46, 3363-3391.

Ek M.B., Mitchell K.E., Lin Y., Rogers E., Grummann P., Koren V., Gayno G., Tarpley J.D. (2003). Implementation of Noah land surface model advances in the National Centers for Environmental Prediction operational mesoscale Eta model. Journal of Geophysical Research 108, 8851.

Engelstaedter S., Tegen I.; Washington R. (2006). North African dust emissions and transport. Earth-Science Reviews 79, 73-100.

Fiedler S., Kaplan M.L., Knippertz P. (2015). Supporting Information for "The importance of Harmattan surges for the emission of North African dust aerosol. Geophysical Research Letters 42, 9495-9504.

Janjić Z.I. (2001). Nonsingular implementation of the Mellor-Yamada level 2.5 scheme in the NCEP Meso model, NCEP Office Note, No.437, 61 pp.

Janjić Z.I. (1996). The surface layer in the NCEP Eta model. Preprints, 11th Conf. on Numerical Weather Prediction, Norfolk, VA, American Meteorological Society, 354–355 pp.

Janjić Z.I. (1994). The step-mountain Eta coordinate model: Further developments of the convection, viscous sublayer, and turbulence closure schemes. Monthly Weather Review 122, 927–945.

Kaplan M.L., Vellore R.K., Lewis J.M., Underwood S.J., Pauley P.M., Martin J.E., Krishnan R. (2013a). Re-examination of the I-5 dust storm. Journal of Geophysical Research-Atmospheres 118, 627-642.

Kaplan M.L., Vellore R.K., Lewis J.M., Underwood S.J., Pauley P.M., Martin J.E., Rabin R.M., Krishnan R. (2013b). Subtropical-polar jet interactions in Southern Plains dust storms. Journal of Geophysical Research-Atmospheres 118, 12893-12914.

Kaplan M.L., Vellore R.K., Marzette P.J., Lewis J.M. (2012). Upstream midtropospheric. circulations enabling leeside (spillover) precipitation over the Sierra Nevada? Leeside adjustments to upslope diabatic heating. Journal of Hydrometeorology 13, 1372-1394.

Klose M., Shao Y. (2013). Large-Eddy Simulation of Turbulent Dust Emission. Aeolian Research 8, 49-58.

Mellor G.L., Yamada T. (1974). A hierarchy of turbulence closure models for planetary boundary layers. Journal of Atmospheric Sciences 31, 1791–1806.

Mlawer E.J., Taubman S.J., Brown P.D., Iacono M.J., Clough S.A. (1997). Radiative transfer for inhomogeneous atmosphere: RRTM, a validated correlated-k model for the longwave. Journal of the Geophysical Research 102, 16663–16682.

Ozer P. (2001). Les lithometeores en region sahelienne, International Journal of Tropical Ecology and Geography 24, 1–317.

Prospero J.M., Lamb P.J. (2003). African droughts and dust transport to the Caribbean: Climate change implications. Science 302, 1024-1027.

Shao Y. (2000).Physics and Modelling of Wind Erosion.Kluwer Academic Norwell, Mass, 393 pp.

Thompson G., Field P.R., Hall W.D., Rasmussen R.M. (2006). A new bulk microphysics parameterization for WRF and MM5, Seventh Weather and Research Forecasting Workshop, National Center for Atmospheric Research, Boulder, CO, NCAR.

Thompson G., Rasmussen R.M., Manning K. (2004). Explicit forecasts of winter precipitation using an improved bulk microphysics scheme. I: Description of sensitivity analysis. Monthly Weather Review 132, 519–542.

Thomson S.W. (1879). On gravitational oscillations of rotating water. Proceedings of the Royal Society of Edinburgh 10, 92–100.

Wang B.(2002). Kelvin Waves.Elsevier Science Ltd.

Washington R., Todd M., Middleton N.J., Goudie A.S. (2003). Dust storm source areas determined by the Total Ozone Monitoring Spectrometer and surface observations. Annals of the Association of American Geographers 93, 297–313.

Wolyn P.G., McKee T. B. (1994). The mountain-plains circulation east of a 2-km high north-south barrier. Monthly Weather Review., 122, 1490-1508.

Zhang F., Koch S.E. (2000). Numerical simulation of a gravity wave event observed during CCOPE. Part II: Wave generation by an orographic density current. Monthly Weather Review 128, 2777–2796.